Mechanism for explosive synchronization of neural networks

B. R. R. Boaretto ⬤, R. C. Budzinski ⬤, T. L. Prado, and S. R. Lopes ⬤*

Departamento de Física, Universidade Federal do Paraná, 81531–980, Curitiba, Paraná, Brazil

Here we investigate the mechanism for explosive synchronization (ES) of a complex neural network composed of nonidentical neurons and coupled by Newman-Watts small-world matrices. We find a range of nonlocal connection probabilities for which the network displays an abrupt transition to phase synchronization, characterizing ES. The mechanism behind the ES is the following: As the coupling parameter is varied in a network of distinct neurons, ES is likely to occur due to a bistable regime, namely a chaotic nonsynchronized and a regular phase-synchronized state in the phase space. In this case, even small coupling changes make possible a transition between them. The onset of ES occurs via a saddle-node bifurcation of a periodic orbit that leads the network dynamics to display a locally stable phase-synchronized state. The presence of this regime is accompanied by a hysteresis loop on the network dynamics as the coupling parameter is adiabatically increased and decreased. The end of the hysteresis loop is marked by a frontier crisis of the chaotic attractor which also determines the end of the coupling strength interval where ES is possible.

I. INTRODUCTION

The possibility of synchronization of coupled oscillators, including those displaying chaotic dynamics, has attracted attention of researchers for many years, once the phenomenon is observed in distinct areas of science, going from life science [1–5] to physics and engineering [6–8]. A particularly important synchronization scenario occurs in coupled neural networks, where a transition from an incoherent state to a phase-synchronized state occurs as the coupling parameter increases. These transitions depict rich dynamics occurring smoothly (a second-order-like phase transition) [9,10] or abruptly (a first-order phase transition) [11–14], not excluding the possibility of the presence of nonstationary intermittent states [15,16].

The understanding of how synchronization regimes occur in neural networks is of fundamental interest since neural synchronization plays a key role in brain functioning and is related to the brain activities such as motor behavior, thoughts, perception, etc. [17–19]. In addition, anomalous synchronization of neurons can generate brain disorders such as seizure behavior creating by epilepsy, Parkinson's disease, and autism [20–26].

Despite the former and more established sense that networks should display a smooth-second-order phase transition as a function of the coupling parameter [10], the observation of abrupt phase transition, often called explosive synchronization (ES), has challenged these conclusions [12,27,28]. In fact, ES has been recently found in many complex networks of chaotic oscillators such as networks under scale-free topology [12–14,29,30]; networks where a microscopic correlation between the frequency of the oscillator and its connectivity degree exists [12]; indirect coupled networks

[31]; networks suffering small topology changes since they can induce shifting in the level of activity propagation of the network, enabling a limited and local activity to turn into a global one [32]; networks depicting a high degree of heterogeneity [13,29,30]. However, other studies contradict the hypothesis of heterogeneity, where neurons which spike regularly with beta rhythms (15–30 Hz) exhibit ES in both random and scale-free networks [33]. Finally, ES can also be induced by the application of disorder terms in the individual dynamics of the oscillators [14].

Here, we focus on the nonlinear mechanism responsible for the presence of explosive phase synchronization of a complex small-world network, where each site is described by nonidentical neurons [34]. The scenario is composed of the presence of mode locking occurring due to the regular dynamics of uncoupled neurons which evolves as the coupling is turned on to a local phase synchronized state. Finite levels of coupling also make possible a second local stable chaotic attractor allowing for a bistability regime and a hysteresis loop.

In such case, complete phase synchronization is not possible but degrees of phase synchronization can be evaluated by using the coherence of neurons initiating their processes of depolarization and repolarization almost together.

Regarding the topology, we use the Newman-Watts route [35] to create a complex network which consists in the addition of nonlocal connections (shortcuts) in a regular network following a given probability. We show that the network exhibits three distinct behaviors for different ranges of nonlocal connection probabilities: For small probabilities, the network does not synchronize, as expected for almost-local-connected networks; for intermediate probabilities, the network depicts ES accompanied by a hysteresis loop as the coupling parameter is varied (a first-order transition); and for larger probabilities, the network synchronizes smoothly as expected for a second-order phase-transition scenario.

*lopes@fisica.ufpr.br

052301-1

In special, for intermediate probabilities, namely the small-world interval, ES occurs due to the presence of a bistable dynamics responsible for the hysteresis of the network dynamics which is associated to the coexistence of a phase-synchronized nonchaotic regime with a chaotic nonsynchronized one. The dynamical mechanisms for the onset and end of the region of ES are given in terms of a saddle-node bifurcation and a frontier crisis [36], respectively. We conclude that this scenario is sufficient for the presence of ES.

The paper is organized as follows: In Sec. II we present the equations which compose the model, as well the details of the topology used for the network simulation; in Sec. III we introduce the Kuramoto order parameter used as the synchronization quantifier; in Sec. IV we discuss the results which support our conclusions that are given in the last section.

II. LOCAL NEURAL DYNAMICS AND THE CONNECTION ARCHITECTURE

We consider a neural network composed of $N = 10\,000$ nodes where the local dynamics is given by the neural model proposed by Chialvo [34]

$$x_{i,t+1} = x_{i,t}^2 \exp(y_{i,t} - x_{i,t}) + k_i + \frac{\varepsilon}{\eta} \sum_{j=1}^{N} e_{i,j} x_{j,t}, \quad (1)$$

$$y_{i,t+1} = a y_{i,t} - b x_{i,t} + c, \quad (2)$$

where $x_{i,t}$ and $y_{i,t}$ are the activation and recovery variables. k_i acts as a constant bias or as a time-dependent additive perturbation [34], which affects the amplitude and frequency of the neurons. Here it is supposed to vary randomly between $[0.03, 0.03 + \sigma]$ from one neuron to another, with σ as the coefficient of neuron dissimilitude, and σ is limited to 0.02 because larger values of k_i lead to a great decrease in the amplitude and increase in the frequency of the neuron. In some cases, it hinders the process of neuronal depolarization. a, b, and c are parameters of the model; η is a normalization factor given by the average number of connections in the network; ε is the coupling strength parameter; and $e_{i,j}$ are elements of the network connection matrix.
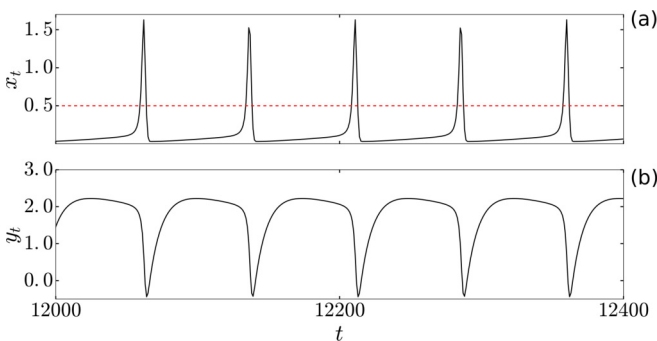

FIG. 1. Dynamical behavior for (a) x_t and (b) y_t of the neural model, Eqs. (1) and (2) for $a = 0.89$, $b = 0.6$, $c = 0.28$, and $k_i = 0.03$. The red dashed line in panel (a) defines a Poincaré surface in $x_0 = 0.5$ used to evaluate the beginning of each spike and the associated phases of the neurons.
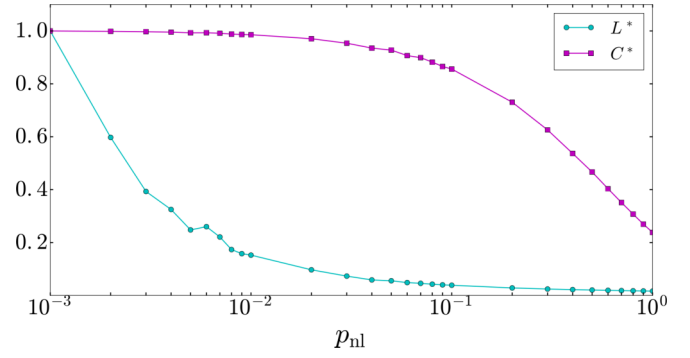

FIG. 2. Normalized values of the average path length (L) (cyan bullet line) and clustering coefficient (C) (magenta square line) as a function of the nonlocal connection probability (p_{nl}) for a second-neighborhood Newman-Watts network of $N = 10\,000$ sites.

Figure 1(a) depicts an example of the evolution of the x_t characterizing the depolarization and repolarization dynamics of an isolated neuron for $a = 0.89$, $b = 0.6$, $c = 0.28$ [34], and $k_i = 0.03$ while Fig. 1(b) shows the respective recovery variable dynamics. For the entire coupling interval used, similar dynamical features are observed for all coupled neurons.

The coupling architecture is characterized by the Newman-Watts route [35]. In this way, we start building the small-world-complex network using four local connected neurons adding a number of randomly distributed nonlocal connections (shortcuts), such that the number of connections in the network is a function of the nonlocal connection probability (p_{nl}) given by [35]

$$n = \underbrace{4N}_{\text{local}} + \underbrace{p_{nl} 4N}_{\text{nonlocal}}. \quad (3)$$

For an intermediate range of p_{nl}, the network has a small average path length but a high clustering coefficient is still preserved, configuring a small-world network regime [35,37].

Figure 2 shows the normalized clustering coefficient $C(p_{nl})$ and the normalized average path length $L(p_{nl})$ of the network as a function of p_{nl}. For $4 \times 10^{-3} \lesssim p_{nl} \lesssim 2 \times 10^{-1}$ the network is considered to be in the small-world regime.

III. SYNCHRONIZATION QUANTIFIER

In order to quantify the phase synchronization of the network, the sequence of spikes of $x_{i,t}$ is used to define a geometric phase of each neuron, $\theta_i(t)$ [38,39]. We define a Poincaré's section at $x_0 = 0.5$ to evaluate the time of the beginning of the spikes. Figure 1(a) depicts a red dashed line which corresponds to this Poincaré's section. Each time $x_{i,t}$ reaches x_0 (upward sense), $\theta_i(t)$ is increased by 2π, such that an interpolation defines the continuous time-varying phase as [38,39]

$$\theta_i(t) = 2\pi \ell_i + 2\pi \frac{t - t_{\ell,i}}{t_{\ell+1,i} - t_{\ell,i}}, \quad t_{\ell,i} \leqslant t < t_{\ell+1,i}, \quad (4)$$

where ℓ_i is the ℓth spike of the ith neuron, t is the current time, and $t_{\ell,i}$ is the time for which the ith neuron starts the ℓth spike.
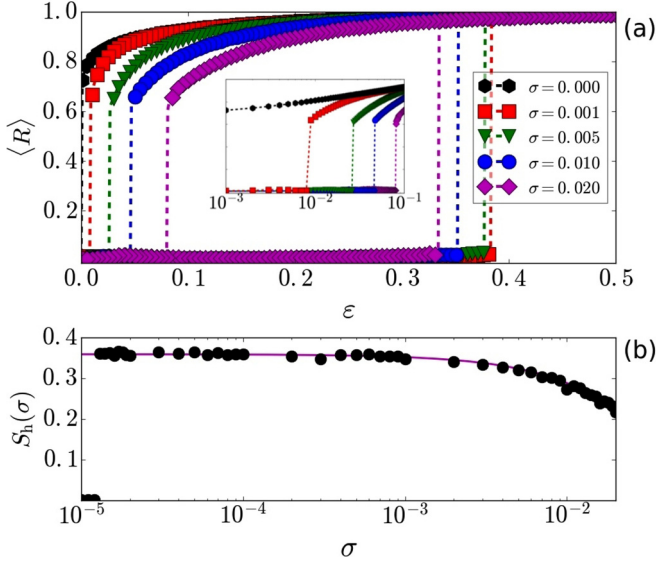
FIG. 3. Mean value of Kuramoto order parameter ($\langle R \rangle$) as a function of the coupling between the neurons for different values of σ [panel (a)] where it is considered $p_{nl} = 0.15$ in the Eq. (3). Vertical dashed lines denote threshold values for ε, $\varepsilon^*(\sigma, p_{nl})$ for the starting and $\varepsilon^\dagger(\sigma, p_{nl})$ for the end of the hysteresis loop. In panel (b) is depicted the hysteresis area described by Eq. (7) as a function of σ.

The synchronization of the network is evaluated by using the modulus of the Kuramoto's order parameter [9,10],

$$R(t) = \left| \frac{1}{N} \sum_{i=1}^{N} e^{i\theta_i(t)} \right|, \quad (5)$$

where θ_i is the phase of the ith neuron at the time t, defined by Eq. (4). $R(t)$ quantifies in a single number the synchronization behavior of the network, since $R \to 0$ represents a complete unsynchronized state and $R \to 1$ represents a complete phase synchronized state. The temporal mean value of the order parameter is defined as

$$\langle R \rangle = \frac{1}{(t_f - t_i)} \sum_{t=t_i}^{t_f} R(t), \quad (6)$$

with t_i and t_f as the initial and final times of the computation of $R(t)$.

IV. RESULTS AND DISCUSSIONS

A. A scenario for explosive synchronization

Considering a small-world representative probability value of $p_{nl} = 0.15$ in Eq. (3), we evaluate the phase synchronization of the network by using $\langle R \rangle$ given by Eq. (6) for $t_i = 150\,000$, $t_f = 200\,000$. The general synchronization behavior of the network as a function of ε is depicted in Fig. 3(a), where five representative values of the coefficient of dissimilitude σ in the interval $0 \leqslant \sigma \leqslant 0.02$ are exemplified. To generate Fig. 3(a), a random initial condition is given to the uncoupled network, evolving it until its asymptotic stable state is reached. Then the coupling parameter is adiabatically increased by $\delta\varepsilon = 0.001$. For the new value of ε, the asymptotic values

obtained by the neuron dynamics (for all variables) for the former value of ε are set as the initial conditions used to evolve the network. Once the network reaches its asymptotic-synchronized monostable state occurring for values of $\varepsilon \gtrsim 0.5$, the same continuation process is carried out but now using a negative step for the variation of ε ($\delta\varepsilon = -0.001$). For all simulations, k_i is uniformly random distributed in the interval $[0.03, \, 0.03 + \sigma]$ generating a nonidentical neural network for $\sigma > 0$.

For the particular case of $\sigma = 0$, the identical and nonchaotic nature of the neurons foments the onset of mode locking for any value of $\varepsilon > 0$ [9] evolving to a phase-locking synchronization as the coupling increases, as observed in the black hexagon curve of the far-left side of Fig. 3(a) and magnified in log-scale in the inset. For this case, the forward and backward increment procedures of ε result in two overlapping curves. For $\sigma > 0$, finite coupling values allow a stable-unsynchronized chaotic state and also a second stable-periodic and partially phase-synchronized state to exist. Increasing ε adiabatically, the continuous process allows the detection of a numerical approximation for the entire interval of stability of the chaotic-unsynchronized state in the ε parameter space as threatened in the following sections.

Such detection is expected since the new initial condition inside the attractor for one value of ε is likely to be in the attraction basin for the next value $\varepsilon + \delta\varepsilon$, even for small volume attraction basins [36].

The stability interval of the chaotic-unsynchronized states is observed in Fig. 3(a) as a set of red, green, blue, and magenta curves showing values of $\langle R \rangle \approx 0$ and occurring for all representative values of $\sigma > 0$. On the other hand, the adiabatically decrease of the values of ε allows the detection of a numerical approximation of the entire interval of stability of a second stable attractor, namely a periodic and phase-synchronized state. This fact configures the bistable region that permits the network of nonidentical neurons to exhibit ES. The ES existence region is demarcated in Fig. 3(a) by dashed-color lines for each value of σ, configuring a hysteresis loop.

In this scenario, no intermediate values of $\langle R \rangle$ are observed at the transition from nonsynchronized to synchronized states, since ES is the result of the spontaneous change of attraction basin of the network when a new value of the coupling strength or even an uncertainty in the neurons' variables are assumed. This scenario starts with the stability gain of the synchronized state extending until the loss of stability of the chaotic attractor.

Figure 3(b) shows results for the numerical values of the hysteresis area $S_h(\sigma)$ as a function of σ, where is performed an integration over the interval $0 < \varepsilon < 0.5$, computed by

$$S_h(\sigma) = \left| \int_{\text{forward}} \langle R \rangle(\varepsilon, \sigma)\, d\varepsilon \int_{\text{backward}} \langle R \rangle(\varepsilon, \sigma)\, d\varepsilon \right|, \quad (7)$$

where "forward" and "backward" refer to the direction assumed for the continuous process of increase and decrease of the coupling parameter, respectively.

For the considered interval of ε, the hysteresis area starts suddenly for finite values of σ decaying linearly (fitted-solid-magenta line) as the dissimilitude increases. Similar behavior is obtained for other values of p_{nl} in the integrated interval.
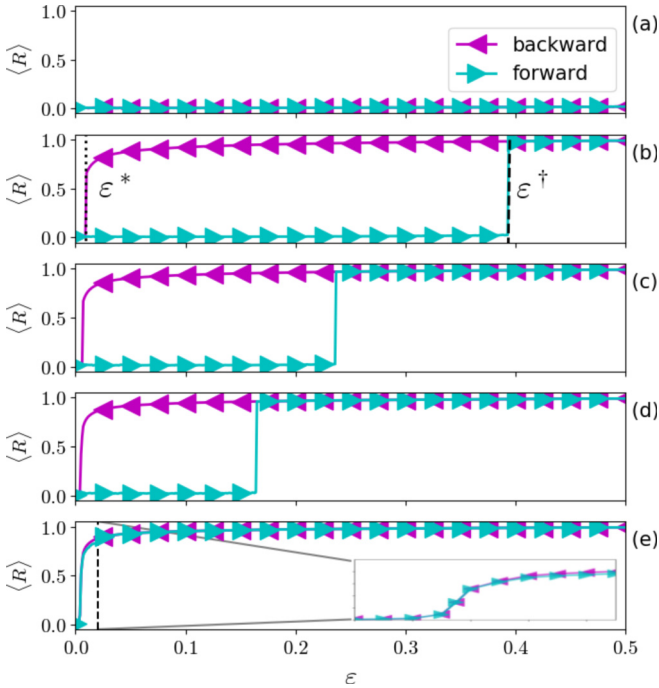
FIG. 4. $\langle R \rangle$ as a function of the coupling strength ε for five distinct nonlocal connection probabilities p_{nl} and a fixed value of $\sigma = 0.001$. The coupling strength is evolved adiabatically ($\delta\varepsilon = 0.001$) in two different directions: forward and backward. (a) For $p_{nl} = 0.10$, the network does not depict phase synchronization. (b) For a larger value of $p_{nl} = 0.15$, a large interval is observed where ES is likely to occur, the vertical dotted (dashed) line represents the transition points of ε^* ($\varepsilon^\dagger$). [(c) and (d)] For $p_{nl} = 0.25$ and $p_{nl} = 0.35$, ES still may exist but for a smaller interval of ε. (e) For larger values of $p_{nl} = 0.45$ the transition from unsynchronized to phase-synchronized state is smooth. Inner panel displays a magnification of the transition region.

The precise mechanism for the stability loss of the chaotic-unsynchronized attractor and the periodic phase-synchronized state is discussed further in the next sections.

Corroborating our initial findings, Fig. 4 shows the results for the continuation algorithm of increase and decrease of the coupling strength and the respective presence of hysteresis for a fixed value of $\sigma = 0.001$ but assuming five values of p_{nl}, (a) 0.10, (b) 0.15, (c) 0.25, (d) 0.35, and (e) 0.45. For a small value of $p_{nl} = 0.10$ [Fig. 4(a)], the hysteresis loop is not observed and only the chaotic-unsynchronized state is stable. In the interval $0.11 \lesssim p_{nl} \lesssim 0.35$, Figs. 4(b)–4(d) depict large hysteresis areas and, consequently, ES is likely to be observed in the hysteresis intervals, in Fig. 4(b) we also delimit the bistability region using a dotted line on $\varepsilon = \varepsilon^*$ and a dashed line on $\varepsilon = \varepsilon^\dagger$. Finally, for large values of $p_{nl} \gtrsim 0.35$, again, no hysteresis is observed and the synchronized state is reached smoothly as expected for a second-order transition, as seen for a representative value of $p_{nl} = 0.45$ in Fig. 4(e).

In general, following our criterion for small-world networks [37,40], the hysteresis area is observed only for a far-right end of the small-world interval of p_{nl} or a little beyond it. As suggested before, the phenomenon of ES as a function of p_{nl} is observed only when a bistable regime for the asymptotic state of the network is present. Again, ES
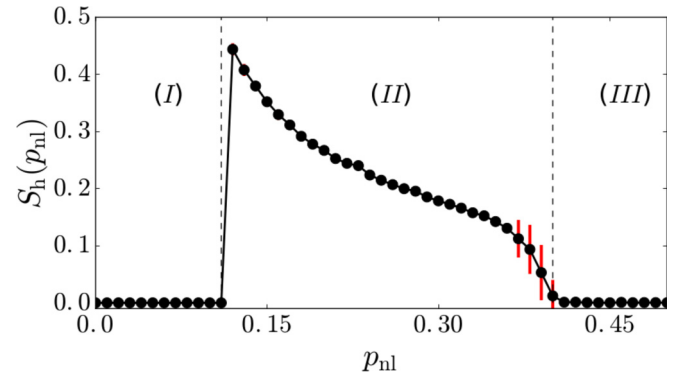

FIG. 5. Numerical results for $S_h(p_{nl})$, which characterize three different scenarios: (I) the network does not show synchronization and only a chaotic-asymptotic states is observed; (II) the network may depict ES as the result of attraction basin changes. At the same time the network displays a hysteresis loop; (III) the networks shows a smooth transition from the unsynchronized state to the synchronized state.

occurs due to the change of attraction basins of both possible locally stable states of the network. Such phenomenon allows a first-order-like transition from an unsynchronized to a phase-synchronized state of the network.

The quantification of the hysteretic behavior of the network as a function of the probabilities p_{nl} may be obtained using, again, Eq. (7), which is rewritten as

$$S_h(p_{nl}) = \left| \int_{forward} \langle R \rangle (\varepsilon, p_{nl})\, d\varepsilon \int_{backward} \langle R \rangle (\varepsilon, p_{nl})\, d\varepsilon \right|. \quad (8)$$

Numerical results for $S_h(p_{nl})$ are shown in Fig. 5, where $\sigma = 0.001$, and the integration is done over the interval $0 < \varepsilon < 0.5$. 20 distinct connection matrices are used to compute the mean value of $S_h(p_{nl})$ and error bars (for some values of p_{nl}, the error bars are smaller than the bullets and so are invisible in Fig. 5). The two dashed lines delimit three regions: (I) where $S_h = 0$ as in Fig. 4(a), for which the network does not synchronize; (II) results for the hysteresis region $0.11 \lesssim p_{nl} \lesssim 0.4$, where the occurrence of hysteresis coinciding with the emergence of a bistable regime for the network dynamics, where a chaotic-nonsynchronized state lives together with a phase-synchronized-periodic state, as seen in Figs. 4(b)–4(d). The hysteresis area is maximum at $p_{nl} = 0.11$ decaying as p_{nl} increases. The decrease of the area is due to a more premature loss of stability of the chaotic attractor as p_{nl} grows; (III), again, $S_h = 0$, but in this case, like Fig. 4(e), the network depicts a smooth-phase transition from the non-phase-synchronized to the phase-synchronized state.

To summarize our results, we have investigate how the hysteretic region varies in the plane (σ, p_{nl}). Figure 6 depicts in color code the critical couplings $\varepsilon^*(\sigma, p_{nl})$ in Fig. 6(a), and $\varepsilon^\dagger(\sigma, p_{nl})$ in Fig. 6(b) which delimits the bistable region. As we increase p_{nl}, the $\varepsilon^\dagger$ decreases; however ε^* varies in an irregular way. Increasing σ, $\varepsilon^\dagger$ decreases and ε^* increases. The black regions reflect the space parameter areas where ES does not occur.
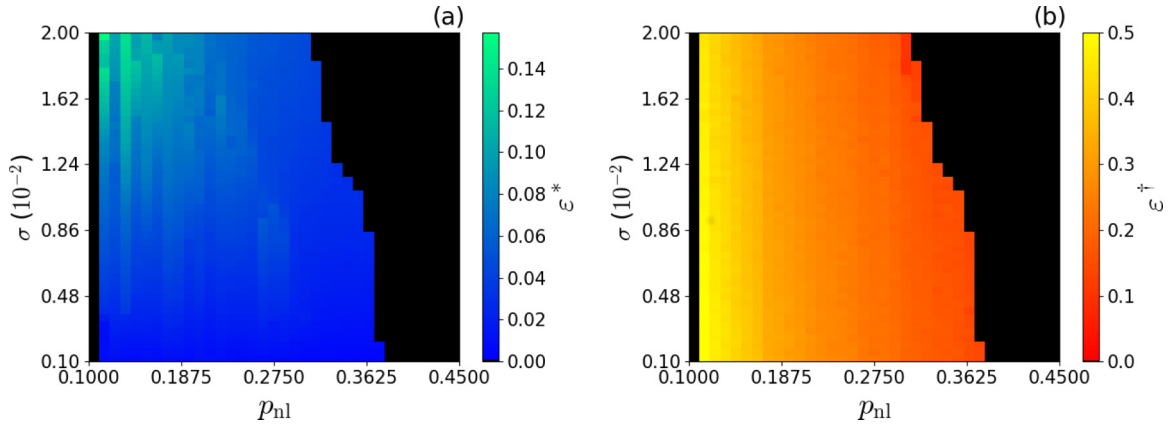
FIG. 6. Numerical results for ε^* (a) and $\varepsilon^\dagger$ (b) on the plane $(\sigma, p_{\mathrm{nl}})$. For a constant σ, increases of p_{nl} lead to decreases of $\varepsilon^\dagger$. However, ε^* varies in a more irregular way. Increases of σ lead to small decreases of $\varepsilon^\dagger$ while ε^* increases. The black regions reflect the space parameter areas where ES does not occur.

B. The dynamical mechanism behind the loss of stability of the chaotic attractor

The physical mechanism responsible for the end of the bistable interval is observed as a transition from an unsynchronized network to a synchronized one, which is described in terms of a route to chaos, namely a frontier crisis [36,41,42] occurring at $\varepsilon \equiv \varepsilon^\dagger(\sigma, p_{\mathrm{nl}})$.

Considering a representative value of $p_{\mathrm{nl}} = 0.15$ and $\sigma = 0.001$, at $\varepsilon^\dagger(\sigma, p_{\mathrm{nl}}) \equiv \varepsilon^\dagger = 0.390 \pm 0.004$, the chaotic attractor collides with its attraction basin boundary. For $\varepsilon > \varepsilon^\dagger$ the attractor no longer exists and is replaced by a chaotic saddle that does not attract trajectories but allows a chaotic transient τ_{crisis} for initial conditions belonging to the former attractor.

Figure 7 depicts the qualitative characteristics of the network mean field,

$$X(t) = \frac{1}{N} \sum_{i=1}^{N} x_{i,t}, \qquad (9)$$

for three values of ε, namely Fig. 7(a) $\varepsilon \lesssim \varepsilon^\dagger$, Fig. 7(b) $\varepsilon \gtrsim \varepsilon^\dagger$, and Fig. 7(c) $\varepsilon > \varepsilon^\dagger$. For $\varepsilon \lesssim \varepsilon^\dagger$ [Fig. 7(a)] the mean field displays the characteristic behavior of a nonsynchronized network, fluctuating perennially around an erratic mean value. For values of $\varepsilon \gtrsim \varepsilon^\dagger$ [Fig. 7(b)] the postcrisis behavior enables long nonsynchronized transient time before the network assumes its asymptotic-synchronized state, inferred here by the large oscillations of the network mean field. For larger values of ε, such that $\varepsilon > \varepsilon^\dagger$ [Fig. 7(c)], the transient nonsynchronized dynamics is quickly lost and the asymptotic-synchronized state is reached.

In order to study the postcrisis behavior, in Fig. 8 we evaluate the average lifetime $\langle \tau_{\mathrm{crisis}} \rangle$ for the chaotic transient of the trajectories inside the chaotic saddle as a function of the distance $|\varepsilon - \varepsilon^\dagger|$.
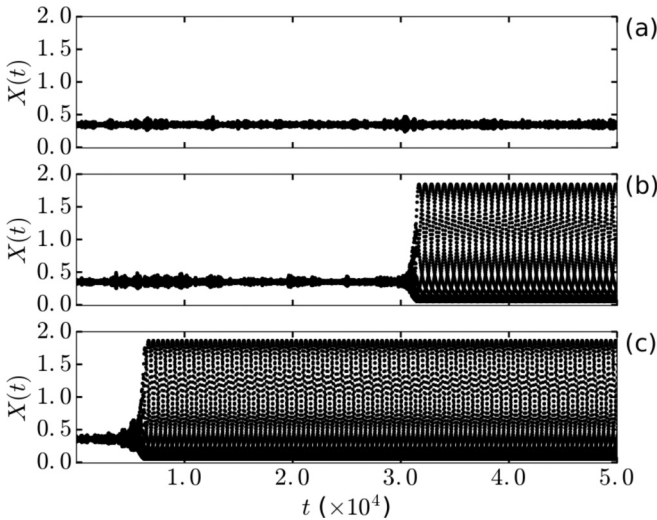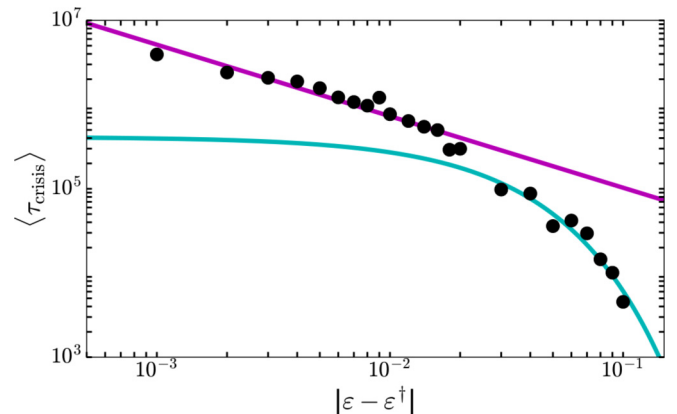

FIG. 7. Evolution of the network mean field [Eq. (9)]. An initial condition embedded in the unsynchronized-chaotic attractor is used to generate all three time series. (a) For $\varepsilon \lesssim \varepsilon^\dagger$, the perennial chaotic state is shown. (b) For $\varepsilon \gtrsim \varepsilon^\dagger$ a long transient chaotic trajectory is the result of the initial dynamics inside the chaotic saddle. (c) For $\varepsilon \gg \varepsilon^\dagger$ the trajectory leads the chaotic saddle after just a few intervals of time. The large oscillations indicate the synchronized behavior.

FIG. 8. Average time for the chaotic transient $\langle \tau_{\mathrm{crisis}} \rangle$ due to the presence of a chaotic saddle for $(\varepsilon \gtrsim \varepsilon^\dagger)$. For small values of $|\varepsilon - \varepsilon^\dagger|$, $\langle \tau_{\mathrm{crisis}} \rangle$ scales as $|\varepsilon - \varepsilon^\dagger|^{-\alpha}$, with $\alpha = 0.85$ as expected for a frontier crisis.

It is expected that $\langle\tau_{\text{crisis}}\rangle$ scales as a power-law function of ε with a characteristic exponent α larger than $1/2$, $\langle\tau_{\text{crisis}}\rangle \propto |\varepsilon - \varepsilon^{\dagger}|^{-\alpha}$ [36,41–43]. To test this scenario, we evolve 50 initial conditions of the system for $\varepsilon \lesssim \varepsilon^{\dagger}$ and for a large interval of time, such that a final suitable set of 50 final conditions inside the chaotic attractor is obtained. Then, we use this set of final conditions as an approximation for initial conditions inside the saddle that replace the chaotic attractor for $\varepsilon \gtrsim \varepsilon^{\dagger}$. Evolving the set of conditions, we compute an approximation for $\langle\tau_{\text{crisis}}\rangle$. Our results are displayed in Fig. 8 and a clear power-law scaling with slope $\alpha = 0.85$ is observed for values of $|\varepsilon - \varepsilon^{\dagger}| < 2 \times 10^{-2}$. For larger values of $|\varepsilon - \varepsilon^{\dagger}|$ the power law is still expected, but in our numerical simulations it is replaced by an exponential law due to the difficult to initialize the system inside the saddle for ε far from $\varepsilon^{\dagger}$.

C. The dynamical mechanism behind the loss of stability of the phase-synchronized attractor

Another important point to discuss is the gain of stability of the synchronized attractor that occurs for a lower coupling parameter $\varepsilon \equiv \varepsilon^*(\sigma, p_{\text{nl}}) < \varepsilon^{\dagger}(\sigma, p_{\text{nl}})$. Again, it is considered a representative value of $p_{\text{nl}} = 0.15$, and $\sigma = 0.001$. We simplify the notation to $\varepsilon^*(\sigma, p_{\text{nl}}) \equiv \varepsilon^*$. Considering an increase of ε, at $\varepsilon = \varepsilon^*$, a saddle-node bifurcation [36] generates a regular, locally stable and phase-synchronized state for the network. So the saddle-node bifurcation, responsible for the birth of the phase-synchronized state, also leads to the onset of the bistable regime and the hysteresis loop, occurring for $\varepsilon^* < \varepsilon < \varepsilon^{\dagger}$. Due to the presence of the unsynchronized-chaotic attractor, before ε^*, the network dynamics converges asymptotically to the unsynchronized-chaotic state. In such a transition, intermittency in the individual dynamics of the neurons is always observed due to the *quasi*stable character of the synchronized state before the saddle-node bifurcation of the periodic-synchronized state [36].

To investigate the details of the saddle-node bifurcation-induced desynchronization that occurs in the "backward" adiabatic evolution of coupling parameter, we consider the behavior of the recovery variable of the model y. Figure 9 depicts the standard deviation (μ) of the maximum values that y assumes as a function of coupling parameter and the neuron index i. In this case, a null value of μ occurring for $\varepsilon > \varepsilon^* = 0.0087 \pm 0.0001$ indicates the periodic and phase-synchronized behavior of neuron, since for each value of ε just one value of y_{max} is observed. On the other hand, higher values of μ indicate a chaotic behavior of the neurons since y_{max} assumes a set of values for each coupling parameter.

For this case, where an adiabatic decrease of the coupling parameter is considered, the regular and synchronized state loses stability for ε lower than the critical value ε^*. In this case, the network dynamics will depict intermittent synchronization for values of $\varepsilon \lesssim \varepsilon^*$. Corroborating this scenario, Fig. 10 shows the typical behavior of three randomly chosen neurons (colored solid lines) for four different values of $\varepsilon < \varepsilon^*$: (a) 0.0087500, (b) 0.008699, (c) 0.008600, and (d) 0.003000, respectively. As observed, the intermittent-synchronized behavior of a typical network neuron is clear, depicting quiescent almost-periodic dynamics interrupted by
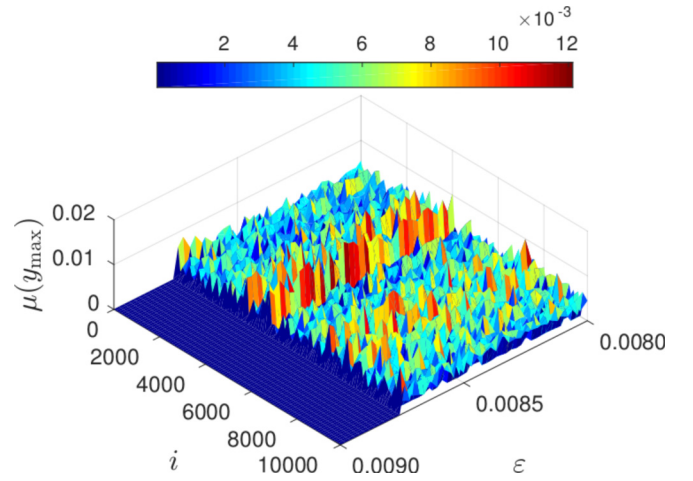

FIG. 9. Standard deviation of the y_{max} as a function of the neurons index and the coupling parameter. Here an adiabatic decrease of the coupling parameter is considered.

chaotic bursts. The further the value of ε is from the critical value ε^* the smaller the intermittent intervals of the almost-synchronized network.

In order to quantify the intermittency, we have computed the mean periodic (phase-synchronized) time τ_{int} as a function of $|\varepsilon - \varepsilon^*|$ [36]. The results are depicted in Fig. 11, which also depicts as a solid line the theoretical fitting observed for type-I intermittency generated by saddle-node bifurcations [36]. As observed, the network behavior fits well the proposed theoretical fitting, supporting our identification of the saddle-
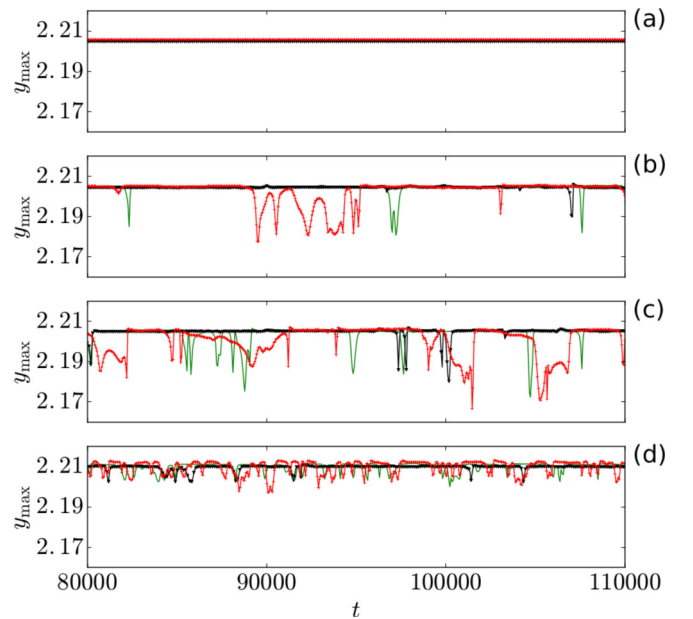

FIG. 10. Temporal dynamics of y_{max} obtained by Eq. (2) for three randomly chosen neurons (colored lines) of the network and distinct values of coupling. (a) A periodic state occurring for $\varepsilon = 0.008750 \gtrsim \varepsilon^*$; (b) intermittent-chaotic bursts occurring just after the saddle-node bifurcation, $\varepsilon = 0.008699 \lesssim \varepsilon^*$; (c) the intermittent-chaotic nature of the neuron for $\varepsilon = 0.008600 < \varepsilon^*$; (d) and the completely chaotic dynamics observed for $\varepsilon = 0.003000 \ll \varepsilon^*$.
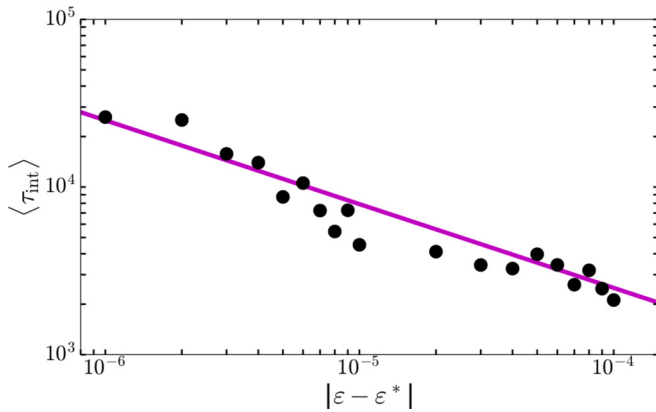
FIG. 11. Saddle-node bifurcation mean intermittent time $\langle \tau_{int} \rangle$ as a function of $|\varepsilon - \varepsilon^*|$ for the type-I intermittency. The theoretical value $\propto |\varepsilon - \varepsilon^*|^{-1/2}$ is plotted as a solid magenta line [36].

node bifurcation as responsible for the onset of the periodic and phase-synchronized state for the network.

V. CONCLUSION

We have simulated a complex network composed of 10 000 distinct neurons modeled by a Chialvo map, Eqs. (1) and (2), under a spike regime to study explosive synchronization phenomena (ES) characterized by a first-order phase transition. We have used the Newman-Watts route to generate a set of small-world networks varying the nonlocal connection prob-

ability and the level of dissimilitude (σ) of the neurons. We have shown that for a range of nonlocal coupling probability and dissimilitude parameter, the network depicts explosive synchronization accompanied by the presence of hysteresis as the coupling parameter is varied.

By using adiabatic increments of the coupling parameter, we have shown that a saddle-node bifurcation rises into the network dynamics as far as σ values are supposed to be bigger than zero. $\sigma > 0$ foments a locally stable-periodic and almost-phase-synchronized state that lives together to a second locally stable-unsynchronized-chaotic attractor generating a bistable regime for the network.

Both attractors survive until the chaotic attractor be destroyed by a frontier crisis. In this scenario, ES is likely to occur in the coupling interval starting from the saddle-node bifurcation and extending to the crisis, since it is the result of a finite probability of the dynamics of the neuron to shift from one attraction basin to another. Such attraction basin changes can be the result of small variations in the coupling parameter, connection probability, or even a finite level of noise in the neuron dynamics.

[1] J. Buck and E. Buck, Sci. Am. **234**, 74 (1976).

[2] J. Buck, Q. Rev. Biol. **63**, 265 (1988).

[3] R. E. Mirollo and S. H. Strogatz, SIAM J. Appl. Math. **50**, 1645 (1990).

[4] J. Jalife, J. Physiol. **356**, 221 (1984).

[5] T. J. Walker, Science **166**, 891 (1969).

[6] A. Arenas, A. Díaz-Guilera, J. Kurths, Y. Moreno, and C. Zhou, Phys. Rep. **469**, 93 (2008).

[7] M. G. Rosenblum, A. S. Pikovsky, and J. Kurths, Phys. Rev. Lett. **76**, 1804 (1996).

[8] B. Blasius, A. Huppert, and L. Stone, Nature **399**, 354 (1999).

[9] Y. Kuramoto, Physica D **50**, 15 (1991).

[10] Y. Kuramoto, *Chemical Oscillations, Waves, and Turbulence*, Vol. 19 (Springer Science & Business Media, Berlin, 2012).

[11] J. Hesse and T. Gross, Front. Syst. Neurosci. **8**, 166 (2014).

[12] J. Gómez-Gardenes, S. Gómez, A. Arenas, and Y. Moreno, Phys. Rev. Lett. **106**, 128701 (2011).

[13] H. Chen, G. He, F. Huang, C. Shen, and Z. Hou, Chaos **23**, 033124 (2013).

[14] P. S. Skardal and A. Arenas, Phys. Rev. E **89**, 062811 (2014).

[15] R. C. Budzinski, B. R. R. Boaretto, T. L. Prado, and S. R. Lopes, Phys. Rev. E **96**, 012320 (2017).

[16] R. C. Budzinski, B. R. R. Boaretto, T. L. Prado, and S. R. Lopes, Phys. Rev. E **99**, 022402 (2019).

[17] E. R. Kandel, J. H. Schwartz, T. M. Jessell, S. A. Siegelbaum, and A. J. Hudspeth, *Principles of Neural Science*, Vol. 4 (McGraw–Hill, New York, 2000).

[18] P. R. Roelfsema, A. K. Engel, P. König, and W. Singer, Nature **385**, 157 (1997).

[19] J. F. Hipp, A. K. Engel, and M. Siegel, Neuron **69**, 387 (2011).

[20] A. Galvan and T. Wichmann, Clin. Neurophysiol. **119**, 1459 (2008).

[21] C. Hammond, H. Bergman, and P. Brown, Trends Neurosci. **30**, 357 (2007).

[22] I. Dinstein, K. Pierce, L. Eyler, S. Solso, R. Malach, M. Behrmann, and E. Courchesne, Neuron **70**, 1218 (2011).

[23] O. V. Popovych and P. A. Tass, Front. Hum. Neurosci. **6**, 58 (2012).

[24] O. V. Popovych and P. A. Tass, Front. Neurol. **5**, 268 (2014).

[25] B. R. R. Boaretto, R. C. Budzinski, T. L. Prado, J. Kurths, and S. R. Lopes, Physica A **497**, 126 (2018).

[26] B. R. R. Boaretto, R. C. Budzinski, T. L. Prado, J. Kurths, and S. R. Lopes, Chaos **28**, 106304 (2018).

[27] X. Zhang, S. Boccaletti, S. Guan, and Z. Liu, Phys. Rev. Lett. **114**, 038701 (2015).

[28] W. Zhou, J. Yang, L. Zhou, and D. Tong, *Stability and Synchronization Control of Stochastic Neural Networks* (Springer, Berlin, 2015).

[29] W. Liu, Y. Wu, J. Xiao, and M. Zhan, Europhys. Lett. **101**, 38002 (2013).

[30] P. Li, K. Zhang, X. Xu, J. Zhang, and M. Small, Phys. Rev. E **87**, 042803 (2013).

[31] A. Sharma, Phys. Lett. A **383**, 2051 (2019).

[32] Z. Wang, C. Tian, M. Dhamala, and Z. Liu, Sci. Rep. **7**, 561 (2017).

[33] M. Khoshkhou and A. Montakhab, Front. Comput. Neurosci. **12**, 59 (2018).

[34] D. R. Chialvo, Chaos Solitons Fract. **5**, 461 (1995).

[35] M. E. J. Newman and D. J. Watts, Phys. Rev. E **60**, 7332 (1999).

[36] E. Ott, *Chaos in Dynamical Systems* (Cambridge University Press, Cambridge, 2002).

[37] D. J. Watts and S. H. Strogatz, Nature **393**, 440 (1998).

[38] M. V. Ivanchenko, G. V. Osipov, V. D. Shalfeev, and J. Kurths, Phys. Rev. Lett. **93**, 134101 (2004).

[39] S. Boccaletti, J. Kurths, G. Osipov, D. Valladares, and C. Zhou, Phys. Rep. **366**, 1 (2002).

[40] S. H. Strogatz, Nature **410**, 268 (2001).

[41] C. Grebogi, E. Ott, and J. A. Yorke, Phys. Rev. Lett. **57**, 1284 (1986).

[42] C. Grebogi, E. Ott, F. Romeiras, and J. A. Yorke, Phys. Rev. A **36**, 5365 (1987).

[43] G. T. Kubo, R. L. Viana, S. R. Lopes, and C. Grebogi, Phys. Lett. A **372**, 5569 (2008).